Title: Spatio-temporal control of DNA replication by the pneumococcal cell cycle regulator CcrZ

Authors: Clement Gallay[1,2,#], Stefano Sanselicio[1,#], Mary E. Anderson[3], Young Min Soh[1], Xue Liu[1], Gro A. Stamsås[4], Simone Pelliciari[5], Renske van Raaphorst[1], Julien Dénéréaz[1], Morten Kjos[4], Heath Murray[5], Stephan Gruber[1], Alan D. Grossman[3], Jan-Willem Veening[1,2,*].

Affiliations:

[1] Department of Fundamental Microbiology, Faculty of Biology and Medicine, University of Lausanne, Biophore Building, CH-1015 Lausanne, Switzerland

[2] Molecular Genetics Group, Groningen Biomolecular Sciences and Biotechnology Institute, Centre for Synthetic Biology, University of Groningen, Nijenborgh 7, 9747 AG Groningen, the Netherlands

[3] Department of Biology, Massachusetts Institute of Technology, Cambridge, MA, USA.

[4] Faculty of Chemistry, Biotechnology and Food Science, Norwegian University of Life Sciences, Ås, Norway

[5] Centre for Bacterial Cell Biology, Biosciences Institute, Newcastle University, Newcastle Upon Tyne NE2 4AX, UK

[#]These authors contributed equally

*Correspondence to Jan-Willem Veening: Jan-Willem.Veening@unil.ch, tel: +41 (0)21 6925625, Twitter handle: @JWVeening.

Abstract:

Most bacteria replicate and segregate their DNA concomitantly before cell division takes place. How these cell cycle events are synchronized to ensure faithful chromosome inheritance is poorly understood. Here, we identified a conserved essential protein in pneumococci and related Firmicutes named CcrZ (for Cell Cycle Regulator protein interacting with FtsZ) that couples cell division with DNA replication. We show that CcrZ from *Streptococcus pneumoniae* localizes at the division site by interacting with the cytoskeleton protein FtsZ and that its absence causes mis-timed and reduced initiation of DNA replication. This work uncovers a new mechanism for the control of the bacterial cell cycle in which CcrZ controls DnaA activity to ensure that the chromosome is replicated at the right time during the cell cycle.

One Sentence Summary:

Identification of CcrZ: a cell cycle regulator that coordinates DNA replication with division in pneumococci and related bacteria.

Main Text

Most organisms have mechanisms ensuring that their genome is replicated and segregated prior to cell division. In many bacterial species, DNA replication and cell division occur concomitantly (*1–3*). Different models emerged from the mid-1900's to explain how bacterial cells handle DNA replication together with cell division in *Escherichia coli* or *Bacillus subtilis* (*4–7*). The current cell-size control model suggests that cells initiate DNA replication independently from their original size, and grow to a constant size independently from their size at birth (adder model) (*8–12*). How cells sense changes in cell size and convert it to trigger replication initiation is not known, but these models imply the existence of regulatory controls (*3*, *13–15*). However, no such cell cycle regulator has been reported yet for bacteria. Specific regulatory models have been proposed for *E. coli* (*16–18*), but these are not applicable to most other organisms, and especially Gram-positive bacteria, that do not contain the proteins proposed to be the regulators. Furthermore, most of the mechanisms known to regulate the initiation of replication and the activity of the replication initiator DnaA in *E. coli* do not exist in other bacteria (*19–23*). This pinpoints a divergence between regulatory systems within bacteria. In line with this notion, changes in DNA replication initiation were shown to alter cell size in *E. coli* and *B. subtilis* but the converse was not true for *B. subtilis* (*24*, *25*). Taken together, current data indicates that bacteria evolved different mechanisms to coordinate their cell cycle events.

Although *E. coli* and *B. subtilis* use different systems for regulating their cell cycle, the way they localize their division site is conserved, as both organisms use a variant of the Min system to prevent polymerization of the tubulin-like protein FtsZ away from mid-cell (*26*, *27*). Both species also have a nucleoid occlusion system (Noc) inhibiting Z-ring formation over the chromosome to prevent "cutting" of the chromosome during cell division (*28*). Together, the Min and Noc systems ensure that cell division and septation occur when both sister chromatids have been fully replicated and segregated. These systems are however not conserved within all bacteria as the Gram-positive opportunistic human pathogen *S. pneumoniae* lacks homologs of the Min and Noc systems (*29*). In contrast to *E. coli* and *B. subtilis*, the pneumococcal Z-ring forms readily over the nucleoid (*29*, *30*). Recently, a pneumococcal specific protein called RocS was identified that might fulfil a similar function as the Noc system by connecting chromosome segregation with capsule production (*31*). Another *S. pneumoniae* specific protein, called MapZ was shown to guide Z-ring formation, analogous to the Min system in other bacteria (*32*, *33*). During cell growth, nascent MapZ rings are pushed apart by septal peptidoglycan synthesis, allowing for FtsZ polymers to continuously assemble at the newly formed septum (*34*). Importantly, the position of the origin of replication (*oriC*) was shown to be crucial for division site selection in *S. pneumoniae* and the origins mark the approximate positions of future division sites (*35*). In *S. pneumoniae*, cell division and DNA replication are thus intimately connected. Critically however, it remains unknown how the cell senses when a new round of replication should be initiated.

We hypothesized that an unknown factor could be responsible for coordination of cell division and DNA replication in the pneumococcus. Using high throughput gene silencing with CRISPRi of all essential genes of *S. pneumoniae* (*36*), we examined proteins leading to DNA content defects upon depletion. Here, we describe the identification of CcrZ, a conserved protein that activates DnaA to trigger initiation of DNA replication. Pneumococcal CcrZ localizes at the division site in a FtsZ-dependent manner and its inactivation leads to division defects. Together,

our findings show that CcrZ acts as a novel spatio-temporal link between cell division and DNA replication in *S. pneumoniae*.

CcrZ is a conserved bacterial cell cycle protein

We previously generated a knock-down library using CRISPRi (clustered regularly interspaced short palindromic repeats interference) targeting 348 conditionally essential genes of the serotype 2 strain *S. pneumoniae* D39V that were identified by Tn-Seq (transposon-insertion sequencing) (*36*). Here, we investigated the function of *spv_0476*, encoding a protein of unknown function that is conserved in most Firmicutes (>30% identity) (fig. S1A). Silencing of *spv_0476* by CRISPRi led to a drastic reduction of the growth rate as well as appearance of anucleate cells as visualized by DAPI staining (Fig. 1, A and B). We renamed SPV_0476 to CcrZ (for Cell Cycle Regulator protein interacting with FtsZ) for reasons explained below. *ccrZ* is in an operon with *trmB*, which encodes a tRNA methyltransferase and this operon structure is conserved across Firmicutes (fig. S1A). To exclude the possibility that the observed phenotypes of *ccrZ* silencing were caused by polar effects on *trmB* expression, we constructed a deletion of *trmB*. This deletion did not lead to any growth defect (fig. S1B left panel). While Tn-seq indicated that *ccrZ* is essential (*36*), we were able to generate a Δ*ccrZ* deletion mutant, although cells grew very slowly. We therefore constructed a depletion of CcrZ by ectopically expressing CcrZ under control of either an IPTG- or a $ZnCl_2$- inducible promoter (P_{lac} and P_{Zn} respectively) and deleted *ccrZ* from its native location ($ccrZ^{-/+}$ and P_{Zn}-$ccrZ^{-/+}$ respectively). Depletion of CcrZ led to a significant growth delay at 37°C and 30°C, confirming the CRISPRi observations (fig. S1B). Immunoblotting using a specific antibody raised against purified CcrZ confirmed CcrZ depletion (fig. S1C).

In line with the CRISPRi observations, DNA staining of cells depleted for CcrZ showed that 20% of cells lacked a nucleoid (Fig. 1C, 442 cells counted). To test whether the *ccrZ*-deletion phenotype was conserved in other Gram-positive bacteria, we silenced *ccrZ* (*SAOUHSC_01866*, here $ccrZ_{Sa}$) in *Staphylococcus aureus* SH1000 using CRISPRi and deleted the *Bacillus subtilis* 168 *ccrZ* homolog (*ytmP*, here $ccrZ_{Bs}$). Upon $CcrZ_{Sa}$ silencing in *S. aureus*, we observed a high proportion of anucleate cells, as well as a delay in growth. In contrast, no obvious phenotypical changes were observed for *B. subtilis* (fig. S1D). Interestingly, the *S. pneumoniae ccrZ* deletion could not be complemented by expression of *ccrZ* from either *B. subtilis* or *S. aureus* as only very small colonies were present on agar plates. In contrast, depletion of *S. aureus* CcrZ was rescued by expression of CcrZ from *B. subtilis* (fig. S1D).

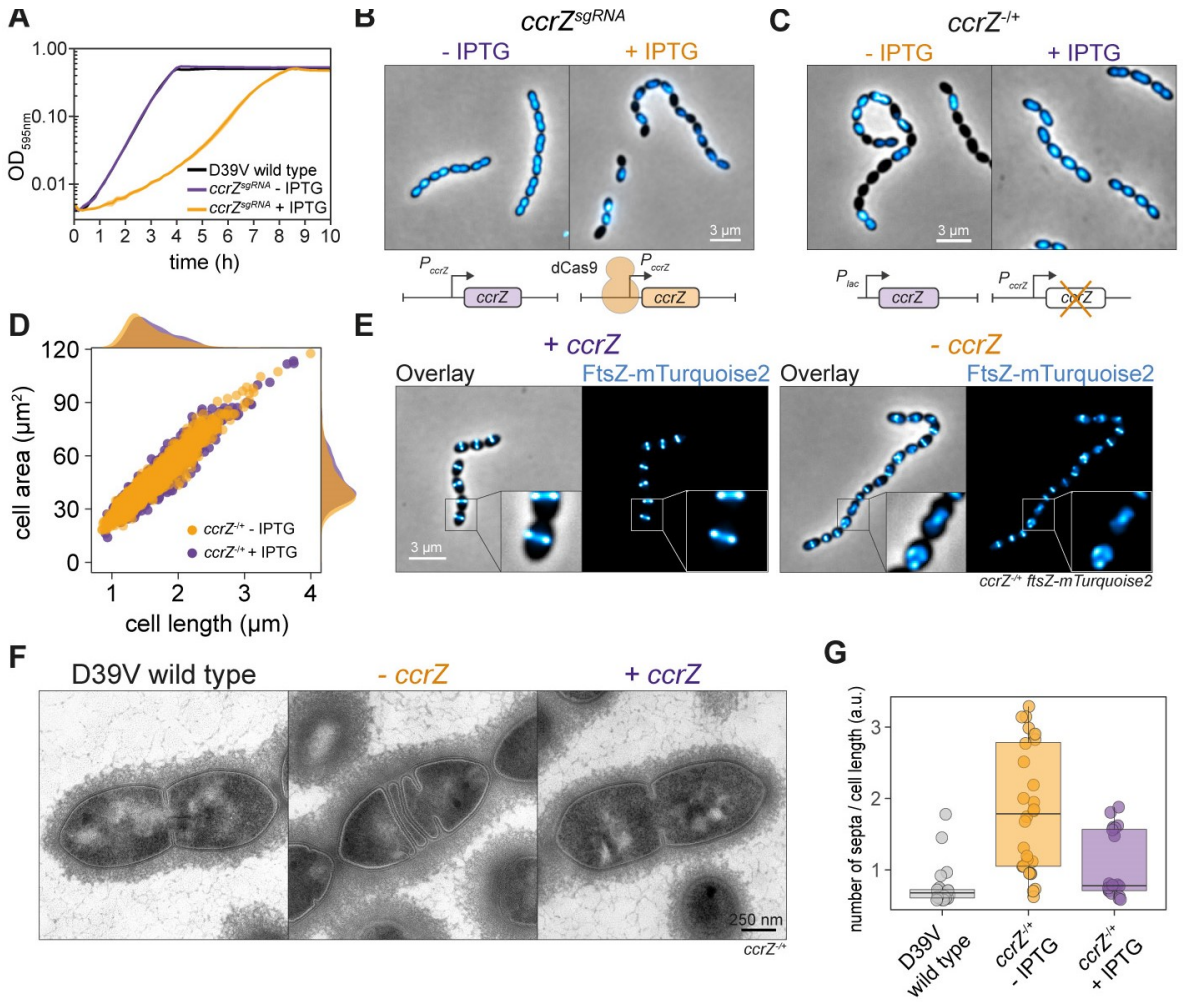

Fig. 1. Depletion of CcrZ leads to anucleate cells and division defects

(**A**) Growth curve of cells with *ccrZ* targeted by CRISPRi (*ccrZ*^{sgRNA} + IPTG) indicates a clear growth defect when *ccrZ* is silenced. (**B**) *CcrZ* silencing leads to appearance of anucleate cells, as visualized by DAPI staining. (**C**) *CcrZ* depletion by ectopic expression via the IPTG-inducible Plac promoter also leads to cells lacking a nucleoid, as observed by DAPI staining. (**D**) Distribution of cell area of *ccrZ*-depleted cells, *ccrZ* depletion leads to a slight decrease in cell length and cell area (P value = 2.2 x 10^{-16}, Wilcoxon rank sum test). (**E**) When a deletion of *ccrZ* is complemented (left panel), FtsZ-mTurquoise2 shows a clear mid-cell localization, while it appears as a blurry signal in several cells upon *ccrZ* depletion (right panel). (**F**) Transmission electron microscopy (TEM) indicates that cells depleted for *ccrZ* form multiple, often incomplete, septa. (**G**) Distribution of number of septa per cell length as determined by TEM for 22 wild type cells, 28 CcrZ-depleted cells and 17 CcrZ-complemented cells (P value = 1 x 10^{-6} for wild type vs *ccrZ*-depleted cells and P value = 0.0013 for *ccrZ*-complemented vs *ccrZ*-depleted cells, Wilcoxon rank sum test with Bonferroni adjustment).

In addition to an increase of the number of anucleate cells, CcrZ depletion in *S. pneumoniae* also led to slight morphological defects and modest changes in cell size when analyzed by phase contrast microscopy (slight decrease in length and increase in width) (Fig. 1D). Polysaccharide capsule production has previously been linked to the pneumococcal cell cycle (*37*), but capsule production was not impacted as the amount of capsule was similar between a CcrZ mutant and

wild type (fig. S1E). To visualize division sites in live cells, we constructed a translational fusion of mTurquoise2 to FtsZ (as the only copy of FtsZ, expressed from its native genetic location), which assembles into distinct rings at new division sites where it recruits the machinery required to form septa (*38*). As shown in Figure 1e, Z-rings were clearly mis-localized upon CcrZ depletion for 3h, with the presence of several aberrant Z-rings in 43% of the cells (Fig. 1E). To obtain more insights into the morphological defects caused by CcrZ depletion and verify that the increased number of septa are not due to the fluorescent protein fused to FtsZ, we employed transmission electron microscopy (TEM) in untagged cells. While not evident by phase contrast microscopy, when *ccrZ* was depleted we observed frequent aberrant septum formation using TEM, in line with the FtsZ localization data, and many cells harbored two (18 %) to four (4 %) septa while only one septum is observed in 91% of wild type cells (Fig. 1, F and G).

S. pneumoniae CcrZ is part of the divisome

As CcrZ seems to be involved in both chromosome biology and cell division, we examined its subcellular localization. Strikingly, immunofluorescence on fixed cells using a CcrZ-specific antibody demonstrated a clear mid-cell localization (fig. S2A). To assess the localization of CcrZ in live cells, we created several functional fusions of a green fluorescent protein to the N-terminus of CcrZ (*gfp-ccrZ*) or a red fluorescent protein to the C-terminus (*ccrZ-mKate2*) and inserted either construct at the native *ccrZ* locus (fig. S1C). Visualization of fluorescently tagged CcrZ by epifluorescence microscopy in live bacteria showed that CcrZ localizes at mid-cell (Fig. 2A). This localization was also conserved in both the TIGR4 and unencapsulated R6 strains (fig. S2B). Interestingly, $CcrZ_{Sa}$ and $CcrZ_{Bs}$ did not localize as clear rings at mid-cell in *S. aureus* and *B. subtilis* (fig. S2B), indicating that the activity and/or localization of CcrZ in these organisms is regulated differently. In order to get higher spatial resolution of *S. pneumoniae* CcrZ, 240 images (16 stacks) on live cells were acquired using 3D-structured illumination microscopy (3D-SIM) and reconstructed to generate a super resolution image and a 3D fluorescence image of GFP-CcrZ. As shown in Fig. 2B and Movie S1, CcrZ forms a patchy ring at mid-cell. Furthermore, time-lapse microscopy showed that CcrZ disassembles from the old septum to assemble at the newly formed division site (Movie S2).

To test whether the mid-cell localization of *S. pneumoniae* CcrZ coincides with FtsZ, we constructed a CcrZ / FtsZ double-labelled strain (*gfp-ccrZ ftsZ-mCherry*). As shown in Fig. 2C, CcrZ co-localized with FtsZ and analysis of still images from exponentially growing cells corroborated this observation (Fig. 2, C, D and E, Movie S3). 3D-SIM also indicated an overlap of GFP-CcrZ and FtsZ-mCherry as well as a similar circular co-localizing pattern at mid-cell (Fig. 2F, fig. S2c and Movie S4).

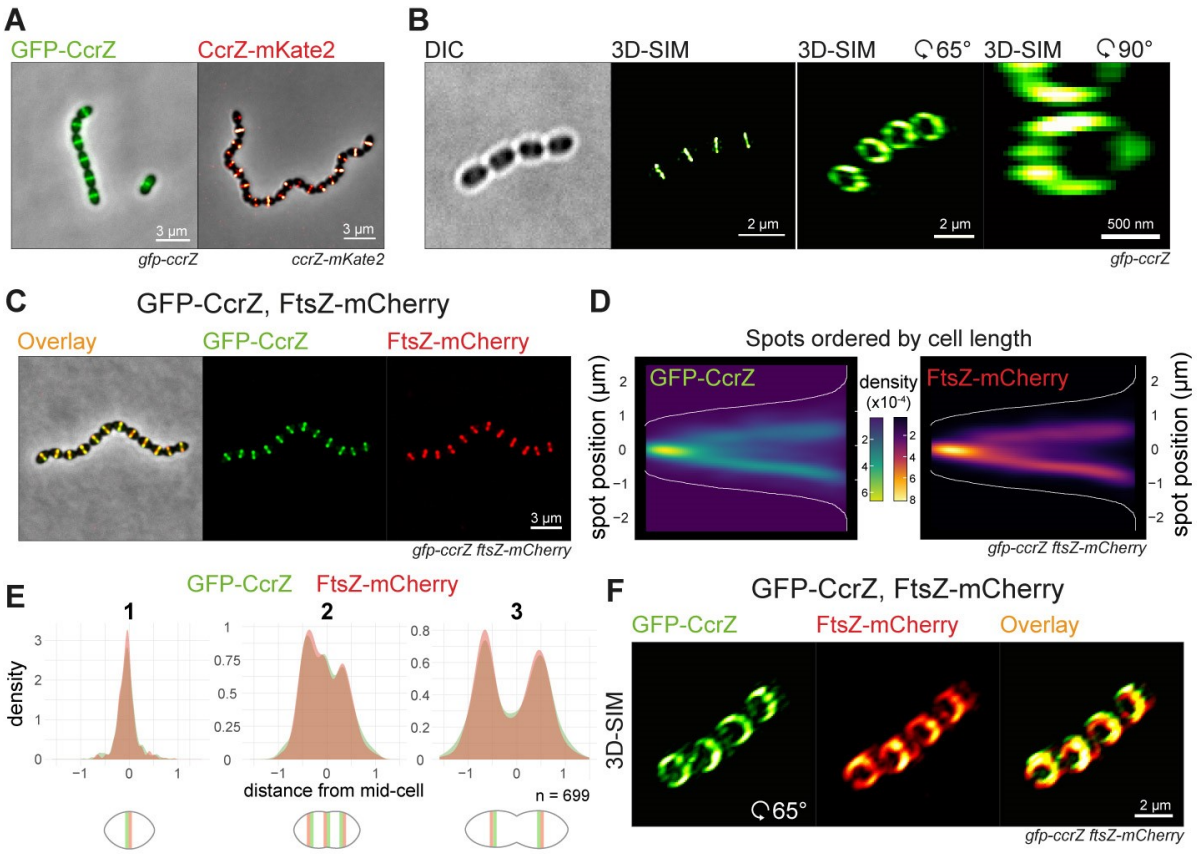

Fig. 2. CcrZ co-localizes with FtsZ at new division sites

(**A**) CcrZ localizes at mid-cell in live wild type *S. pneumoniae* cells as observed by epifluorescence microscopy of GFP-CcrZ and CcrZ-mKate2. (**B**) 3D-SIM of GFP-CcrZ and reconstructed volume projection (right) indicate that CcrZ forms a patchy ring at mid-cell. (**C**) GFP-CcrZ and FtsZ-mCherry co-localize in wild type cells. (**D**) Localization signal of GFP-CcrZ and FtsZ-mCherry in 699 cells of a double labelled *gfp-ccrZ ftsZ-mCherry* strain, ordered by cell length and represented by a heatmap. (**E**) GFP-CcrZ and FtsZ-mCherry co-localize during the entire cell cycle, as visualized when signal localization over cell length is grouped in three quantiles. (**F**) 3D-SIM co-localization of GFP-CcrZ and FtsZ-mCherry shows a clear co-localizing ring with identical patchy pattern. Note that for clarity, we did not correct for chromatic shift in the overlay.

Prediction of CcrZ's topology using TMHMM (*39*) did not indicate the presence of a transmembrane domain; CcrZ's septal localization might then rely on another partner. To identify possible partners, we purified GFP-CcrZ expressed from *S. pneumoniae* and untagged cytosolic sfGFP as a control using anti-GFP nanobodies (GFP-Trap) without cross-linking, and directly analyzed the purified fraction by liquid chromatography-tandem mass spectrometry (LC-MS/MS). Interestingly, we found an enrichment (> 5-fold change) for several proteins from the divisome (*e.g.,* FtsZ, PBP2X and EzrA) (Table S1). To determine which of the candidates might interact directly with CcrZ, we used the NanoBit complementation reporter assay (*40*, *41*), which uses an enhanced luciferase separated into two different fragments (large bit (LgBit) and small bit (SmBit), respectively). Fusion of two different interacting proteins to each fragment can restore the activity of the luciferase and, in presence of a furimazine-based substrate, produce light (*40*). Accordingly,

we fused the C-terminal extremity of CcrZ to LgBit (*ccrZ-LgBit*) and putative partners to SmBit and integrated the different constructs at their respective loci under native control. We also fused SmBit to other proteins known to localize at the septum (Cps2E, FtsA, FtsW and ZapA), or to the highly abundant histone-like protein HlpA localizing at the nucleoid and used a strain expressing both HlpA-LgBit and HlpA-SmBit as a positive control of interaction. After addition of the substrate, we could detect a strong and reproducible signal when FtsZ was fused to SmBit and CcrZ to LgBit, as well as a weaker signal for FtsA, EzrA and ZapA, and no detectable signal for any of the other proteins (Fig. 3A). This result indicates that FtsZ and CcrZ in *S. pneumoniae* are in very close proximity in space. Interestingly, using a strain expressing both CcrZ-LgBit and CcrZ-SmBit, a weak signal was observed indicating that CcrZ might also self-interact (Fig. 3A).

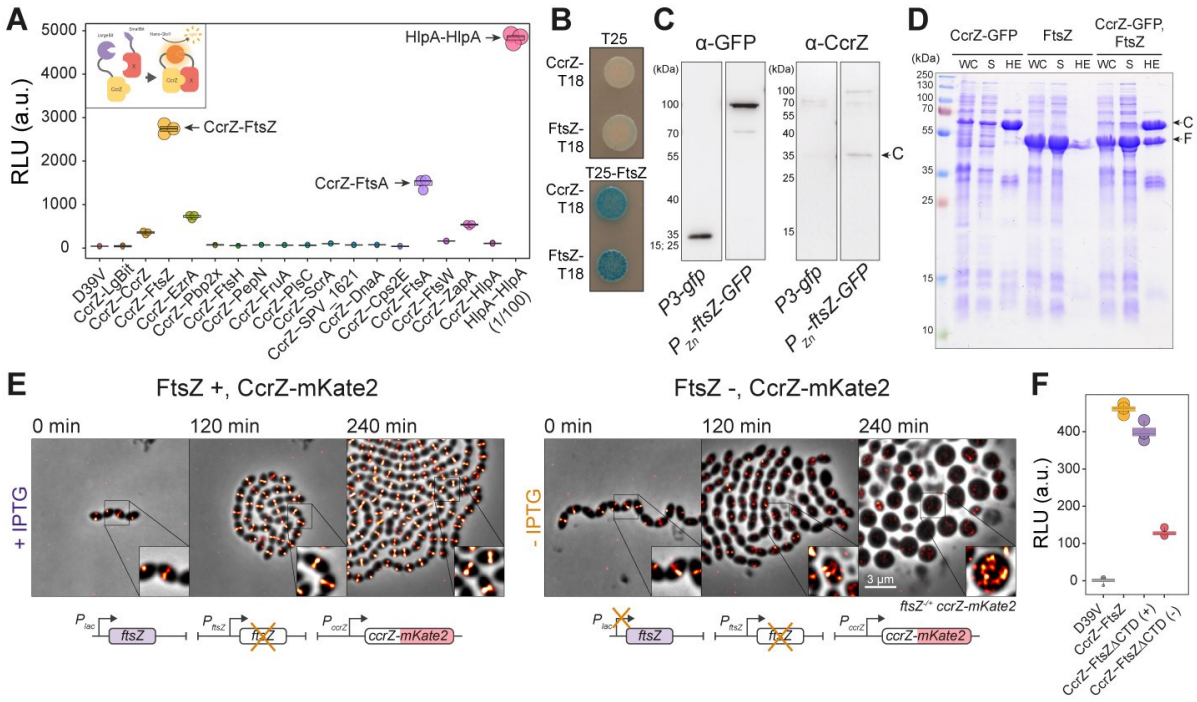

Fig. 3. CcrZ directly interacts with FtsZ

(**A**) Split-luciferase assay using several combinations with CcrZ-LgBit reveals that CcrZ and FtsZ are in very close proximity, as indicated by a high luminescence signal. FtsA, EzrA and ZapA, all three interacting directly with FtsZ, also gave a slight signal. *hlpA-LgBit hlpA-SmBit* (HlpA-HlpA), here diluted 100 times, is used as positive control. Each dot represents the average of 15 measurements of a technical replicate, with the size of the dot representing the SEM. (**B**) FtsZ-CcrZ interaction confirmation by bacterial two-hybrid assay. T25 is the empty vector pST25 and T25-FtsZ corresponds to vector pST25-FtsZ used in combination with pUT18-CcrZ (CcrZ-T18) and pUT18-FtsZ (FtsZ-T18). (**C**) Affinity purification of FtsZ-GFP from *S. pneumoniae* cells (2nd lane) also pulls down untagged CcrZ (4th lane). Purification of GFP alone (first lane) did not pull CcrZ down (3rd lane). (D**A**) FtsZ from *S. pneumoniae* expressed in *E. coli* co-purifies with $CcrZ_{Sp}$-GFP by affinity purification. WC: whole cell extract, S: supernatant, HE: heat eluted products, C: CcrZ, F: FtsZ. (**E**) Epifluorescence time-lapse microscopy of CcrZ-mKate2 at 37°C in presence (left panel) or absence (right panel) of FtsZ. When FtsZ amounts are reduced, cells increase their size and CcrZ is de-localized from mid-cell. (**F**) Split-luciferase assay using a combination of CcrZ-LgBit with SmBit fused to FtsZ wild type or to a mutant of FtsZ lacking the last 17 C-terminal residues (FtsZΔCTD: FtsZ I403_*420del-SmBit) when a second copy of FtsZ is expressed (+) or depleted (-).

To confirm the observed interaction with FtsZ, we used a bacterial two-hybrid assay in *E. coli* (*42*). Again, we observed a robust interaction between CcrZ and FtsZ, while T25-FtsZ did not interact with the empty vector alone, strongly suggesting that CcrZ directly binds to FtsZ (Fig. 3B). Co-immunoprecipitation of FtsZ-GFP from *S. pneumoniae* cells confirmed the *in vivo* interaction with CcrZ (Fig. 3C). Affinity purification of $CcrZ_{Sp}$-GFP when over-expressing $FtsZ_{Sp}$ in *E. coli* also confirmed this interaction as we were able to co-purify FtsZ in large amounts (Fig. 3D). Using size-exclusion chromatography we were able to determine that FtsZ:CcrZ form a complex with a 1:1 ratio. To test whether the localization of CcrZ depends on FtsZ, we constructed a strain expressing CcrZ-mKate2 as well as a second copy of FtsZ under the control of an IPTG-inducible promoter and deleted the native *ftsZ* gene ($ftsZ^{-/+}$). As expected, FtsZ depletion led to aberrant cell morphology and, consistent with a FtsZ-CcrZ interaction, CcrZ-mKate2 was rapidly mis-localized and the signal was spread throughout the cytoplasm (Fig. 3E, Movie S5). FtsZ is known to interact with several septal proteins (*e.g.,* FtsA and ZapA) through a short sequence of 17 residues at its C-terminal extremity (*43*). To determine whether CcrZ also interacts with these residues, we deleted the last 17 amino acids of native FtsZ (FtsZΔCTD: FtsZ I403_*420del) and fused it to SmBit. Since this mutation is lethal, we expressed a second ectopic wild type copy of FtsZ under control of an IPTG-inducible promoter. When FtsZ wild type was expressed, the luminescence intensity observed for CcrZ- FtsZΔCTD interaction was slightly weaker than for CcrZ-FtsZ (Fig. 3F). When FtsZ wild type was depleted for 1h30, the signal significantly decreased, although FtsZΔCTD was still expressed, indicating a reduction in CcrZ-FtsZΔCTD interaction (Fig. 3F). In total, we conclude that CcrZ localizes to new division sites via a direct interaction with the C-terminus of FtsZ.

CcrZ controls DNA replication

As shown in Fig. 1C, when cells are depleted for CcrZ, a large proportion of cells become anucleate. To investigate the consequences of lack of CcrZ on chromosome segregation in live cells, we introduced a translational fluorescent fusion of HlpA (*44*) and deleted *ccrZ*. Localization of HlpA-mKate2 in this slow growing Δ*ccrZ* mutant showed similar results to DAPI stained cells depleted for CcrZ and we observed that 19 % of cells lacked a nucleoid signal (fig. S3A, 4855 cells counted). Time-lapse imaging indicated that cells with defective DNA content had either no DNA at all or chromosomes "guillotined" during septum closure suggesting reduced nucleoid occlusion control in Δ*ccrZ* (Fig. 4A, Movie S6). We also co-localized FtsZ-CFP with HlpA-mKate2 while depleting CcrZ for a short period of time (2h). Interestingly, we observed many cells with a chromosome localized at only one half of the cell, at one side of the Z-ring (Fig. 4B). The absence of DNA in the other half of the cell could be explained by defective DNA segregation, by impaired replication or by DNA degradation.

When attempting to make clean *ccrZ* deletions, in addition to small colonies typical of slow growing mutants, there were also spontaneous large, wild type-sized colonies. Growth analysis of cells from three of these large colonies ($ccrZ^{supp1-3}$) showed that cells behaved like wild type and DAPI staining revealed a restoration of wild type DNA content (Fig. 4, C and D). To verify whether these wild type-like phenotypes were caused by suppressor mutations, the genomes of these fast-growing strains were sequenced. All three strains still contained the *ccrZ* deletion and, in addition, contained a single nucleotide polymorphism elsewhere in the genome (Fig. 4E). Two missense mutations were found in *dnaA* (DnaA-Q247H and DnaA-S292G) and one nonsense

mutation in *yabA* (YabA-E93*). Since DnaA promotes initiation of DNA replication and YabA hampers it by preventing interaction of DnaA with DnaN (*45*), we wondered whether the frequency of DNA replication initiation was changed in a *ccrZ* mutant.

To test this hypothesis, we quantified the copy number ratio between chromosomal origin and terminus regions (*oriC/ter* ratios) using real-time quantitative PCR. In a wild type situation, during exponential growth, the *oriC/ter* ratio varies between 1.3 – 1.8, as most cells have started a round of DNA replication (note that in contrast to *E. coli* and *B. subtilis*, multifork replication does not occur in *S. pneumoniae*) (*46*). Remarkably, depletion of CcrZ resulted in a significantly decreased DNA replication initiation rate with an *oriC/ter* ratio of 1.1 vs 1.8 for complemented cells (P value < 0.05) (Fig. 4F). Interestingly, the same observation was made for both *B. subtilis* and *S. aureus*, where deletion or depletion of CcrZ caused a clear reduction in *oriC/ter* ratios (Fig. 4G). As the identified *ccrZ*-bypass mutations were found in DNA replication initiation regulators, we tested whether they would restore the *oriC/ter* ratio in a fresh *ccrZ* deletion background in *S. pneumoniae*. Indeed, the *oriC/ter* ratios for Δ*ccrZ dnaA-S292G,* Δ*ccrZ dnaA-Q247H* and for *yabA-E93** (*ccrZ*^{supp3}) were like wild type (Fig. 4, H and I).

The point mutation found in *yabA* causes premature translation termination at the C-terminus of YabA. When *yabA* alone was replaced by an antibiotic resistance cassette, we observed an increase of replication initiation as well as a reduced growth rate; but when *ccrZ* was co-deleted, wild type like growth and a wild type *oriC/ter* ratio was restored (Fig. 4, I and J). DnaA suppressor mutations were located in the AAA+ ATPase domain of DnaA (*47*) (fig. S3B) and it was previously reported that specific mutations in this domain could increase the initiation rate in *B. subtilis* (*48*). To determine if those mutations alone were able to induce over-initiation, we inserted each *dnaA* mutation into a wild type background strain. Marker frequency analysis detected an increase in the *oriC/ter* ratio for both *dnaA* alleles (Fig. 4K). We conclude that mutations that increase the rate of initiation of DNA replication can rescue the Δ*ccrZ* phenotype.

To gain additional insights into CcrZ function, we performed a genome-wide genetic interaction screen in cells depleted for CcrZ using CRISPRi-seq (*49*) (Fig. 4L). This technique relies on the expression of dCas9, controlled by an anhydrotetracycline (aTc) -inducible promoter, and constitutive expression of a specific sgRNA that together form a roadblock for RNAP and thereby downregulated transcription of the targeted operon. We created a CRISPRi library by transforming *S. pneumoniae* P_{tet}*-dCas9,* P_{lac}*-ccrZ,* Δ*ccrZ* with 1,499 different sgRNAs targeting 2,111 out of 2,146 genetic elements of *S. pneumoniae*. The resulting library was grown in presence or absence of aTc to repress, or not, every operon, and in presence or absence of IPTG to express or deplete *ccrZ*, and the sgRNAs were then sequenced by Illumina sequencing. If an operon becomes more essential in a *ccrZ*-depletion background than in an induced *ccrZ* background, the corresponding sgRNA will therefore be under-represented. After analyzing the fold change for every sgRNA between *ccrZ*-depletion and *ccrZ*-complementation, we found an enrichment of sgRNAs targeting the operon of YabA / HolB (*tmk-holB-yabA-spv_0828*), indicating that depletion of this operon becomes beneficial for growth of Δ*ccrZ* (Fig. 4M and Data S1). This confirms that deletion of YabA can complement a *ccrZ* deletion. Interestingly, we also found that inactivation of two genes coding for FtsK and RocS, worsened the fitness of a *ccrZ* mutant. RocS is a regulator of chromosome segregation in *S. pneumoniae* interacting with the DNA and the chromosome partitioning protein ParB (*31*) and FtsK is thought to couple segregation of the

chromosome terminus during cell division (*50*). These interactions reinforce a role of CcrZ in chromosome integrity and replication and that CcrZ acts in a distinct pathway from these chromosome segregation factors. Finally, to test whether the midcell localization of CcrZ is important for well-timed replication of the chromosome, we abrogated CcrZ's mid-cell localization by depleting cells for FtsZ (Fig. 3E). After 2h of FtsZ depletion, chromosomal DNA was isolated and *oriC*/*ter* ratios were determined. This showed that upon mis-localization of CcrZ, cells under replicate (Fig. 4N).

CcrZ is a conserved regulator of DnaA

The results so far suggest that the division defects observed in the absence of CcrZ are due to perturbed Z-ring formation caused by under-replication of the chromosome. To examine whether disruption of DNA replication in general could lead to division defects similar to those of a *ccrZ* mutant, we took advantage of a thermosensitive *dnaA* mutant ($dnaA^{TS}$) in which DNA replication initiation is drastically reduced when cells are grown at the non-permissive temperature (40°C) (*31*). As expected, when shifted to the non-permissive temperature, many cells were anucleate (fig. S4A). Strikingly, localization of FtsZ-mTurquoise2 in the $dnaA^{TS}$ strain at 40°C phenocopied the Δ*ccrZ* mutant, and FtsZ was frequently mis-localized (Fig. 5A). Examination by time-lapse microscopy following a temperature shift from 30°C to 40°C showed that FtsZ-mTurquoise2 mis-localization occurs after four to five generations (Movie S7). Furthermore, examination by TEM at 40°C showed many cells with aberrant septa like CcrZ-depleted cells (Fig. 5B). As DnaA inactivation leads to strikingly similar phenotypes, these data are consistent with the idea that CcrZ exerts a control on DNA replication initiation.

To test whether CcrZ controls DNA replication via regulating DnaA activity, we made use of the fact that a *B. subtilis* $\Delta ccrZ_{Bs}$ mutant also under-initiates (Fig. 4G) and a strain was constructed in which DNA replication was driven in a RepN-dependent manner (from a plasmid origin of replication *oriN*) rather than from DnaA-dependent initiation (from *oriC*). This showed no significant *ori*-*ter* ratio differences when *ccrZ* was deleted (Fig. 5C), suggesting that CcrZ is an activator of DnaA-dependent initiation of replication in *B. subtilis*. We therefore tested whether CcrZ interacts directly with DnaA to trigger DNA replication and employed bacterial two-hybrid assays and the Split-luc system using pneumococcal CcrZ and DnaA (Fig. 3A and fig. S4B). However, none of these assays revealed a direct protein-protein interaction. In line with our genetic data, we also did not find a direct interaction of CcrZ with YabA, while YabA clearly interacts with DnaA (fig. S4C). It is still possible that CcrZ interacts directly with DnaA, but that we cannot detect it with these assays. Alternatively, another factor might be required for CcrZ's function or CcrZ indirectly affects the activity of DnaA in replication initiation.

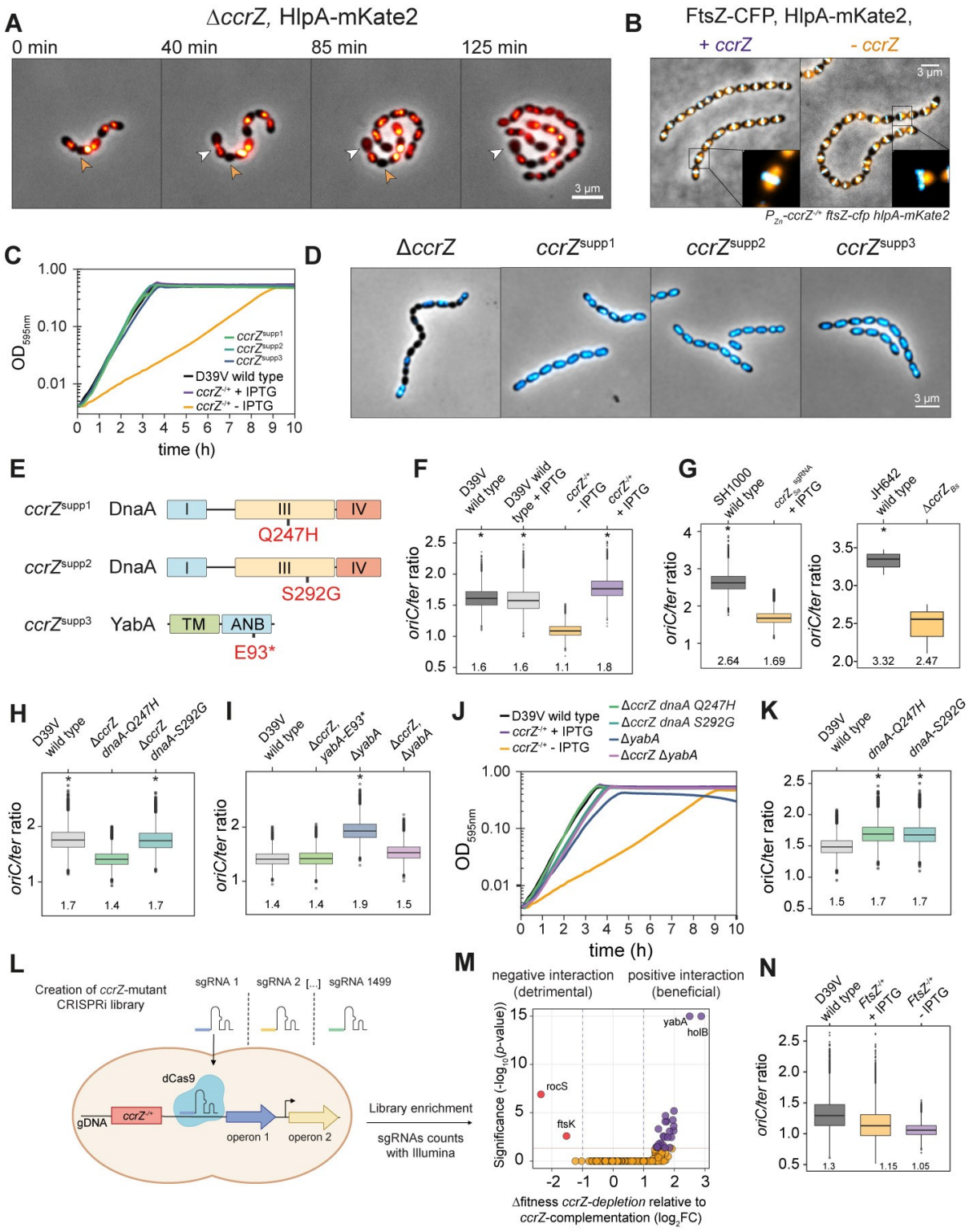
A
ΔccrZ, HlpA-mKate2
0 min
40 min
85 min
125 min
3 µm
B
FtsZ-CFP, HlpA-mKate2,
+ ccrZ
- ccrZ
3 µm
P_Zn-ccrZ-/+ ftsZ-cfp hlpA-mKate2
C
OD595nm
time (h)
ccrZsupp1
ccrZsupp2
ccrZsupp3
D39V wild type
ccrZ-/+ + IPTG
ccrZ-/+ - IPTG
D
ΔccrZ
ccrZsupp1
ccrZsupp2
ccrZsupp3
3 µm
E
ccrZsupp1 DnaA I III IV Q247H
ccrZsupp2 DnaA I III IV S292G
ccrZsupp3 YabA TM ANB E93*
F
D39V wild type
D39V wild type + IPTG
ccrZ-/+ - IPTG
ccrZ-/+ + IPTG
oriC/ter ratio
1.6 1.6 1.1 1.8
G
SH1000 wild type
ccrZ-Bs sgRNA + IPTG
JH642 wild type
ΔccrZ-Bs
oriC/ter ratio
2.64 1.69
3.32 2.47
H
D39V wild type
ΔccrZ dnaA-Q247H
ΔccrZ dnaA-S292G
oriC/ter ratio
1.7 1.4 1.7
I
D39V wild type
ΔccrZ, yabA-E93*
ΔyabA
ΔccrZ, ΔyabA
oriC/ter ratio
1.4 1.4 1.9 1.5
J
D39V wild type
ccrZ-/+ + IPTG
ccrZ-/+ - IPTG
ΔccrZ dnaA Q247H
ΔccrZ dnaA S292G
ΔyabA
ΔccrZ ΔyabA
OD595nm
time (h)
K
D39V wild type
dnaA-Q247H
dnaA-S292G
oriC/ter ratio
1.5 1.7 1.7
L
Creation of ccrZ-mutant CRISPRi library
sgRNA 1
sgRNA 2
[...]
sgRNA 1499
dCas9
gDNA
ccrZ-/+
operon 1
operon 2
Library enrichment
sgRNAs counts with Illumina
M
negative interaction (detrimental)
positive interaction (beneficial)
yabA
holB
rocS
ftsK
Significance (-log10(p-value))
Δfitness ccrZ-depletion relative to ccrZ-complementation (log2FC)
N
D39V wild type
FtsZ-/+ + IPTG
FtsZ-/+ - IPTG
oriC/ter ratio
1.3 1.15 1.05

Fig. 4. CcrZ-depleted cells under-replicate

(**A**) Time-lapse microscopy of HlpA-mKate2 at 30°C in a Δ*ccrZ* mutant shows several cells with defective DNA content. Orange arrows indicate a cell with no nucleoid after cell division; white arrows indicate a cell with "guillotined" DNA. (**B**) Co-localization of FtsZ-CFP and HlpA-mKate2 when depleting *ccrZ* indicates that several cells have a nucleoid located only on one side of the Z-ring. (**C**) Three isolated *ccrZ* mutants ($ccrZ^{supp1-3}$) restore wild type growth to Δ*ccrZ*. (**D**) DAPI staining of the three selected *ccrZ* suppressors mutants shows a restoration of DNA content. (**E**) Schematic representation of the localization of suppressor mutations in the domain III of DnaA and in the DnaA/DnaN binding motif (ANB) of YabA. TM: tetramerization domain. (**F**) *oriC/ter* ratios as determined by RT qPCR for D39V wild type and *ccrZ* depleted cells. Average values are indicated under the boxes. *ccrZ* depletion leads to a clear reduction in *oriC/ter* ratio. (**G**) *oriC/ter* ratios for *S. aureus* upon $ccrZ_{Sa}$ depletion (left) and for *B. subtilis* with $ccrZ_{Bs}$ deletion (right). (**H**) *oriC/ter* ratios of strains with *dnaA* mutations re-inserted into a Δ*ccrZ* background show that these mutations restore replication initiation rates. (**I**) *yabA* deletion leads to an increase in *oriC/ter* ratios, while suppressor mutation $ccrZ^{supp3}$ (Δ*ccrZ*, *yabA-E93**) as well as co-deletion of *yabA* together with *ccrZ* (Δ*yabA* Δ*ccrZ*) restore a wild type ratio. (**J**) While *yabA* deletion alters the growth rate, a Δ*yabA* Δ*ccrZ* double mutant grows like wild type. *dnaA Q247H* and *dnaA S292G* mutation also restore a wild type rate in a Δ*ccrZ* mutant. (**K**) *dnaA* mutation in a wildtype background increases the *oriC/ter* ratios. See Methods for statistical tests. (**L**) Schematic overview of CRISPRi-seq. *ccrZ*-depletion strain ($ccrZ^{-/+}$) was transformed with 1,499 different sgRNAs targeting 2,111 genetic elements of *S. pneumoniae*. These sgRNAs are expressed constitutively. The resulting library is then grown in presence or absence of inducer for production of dCas9 and the genomic DNA isolated. After sequencing of the sgRNA region, reads counts are compared between *ccrZ* depleted induced and complemented induced, indicating which sgRNAs were enriched or deprived. This fold change directly informs whether the gene targeted by the sgRNA becomes more (beneficial) or less (detrimental) essential in a specific genetic background. (**M**) CRISPRi-seq of *ccrZ*-depletion vs *ccrZ*-expression shows a positive interaction between *ccrZ* and *yabA / holB* (these two genes are in the same operon) and a negative interaction between *ccrZ* and *ftsK / rocS*. (**N**) *oriC/ter* ratios for FtsZ depletion strain ($FtsZ^{-/+}$) shows a reduced ratio when FtsZ is depleted (- IPTG) compared to when it is complemented (+ IPTG).

CcrZ's conserved residues are essential for its function

S. pneumoniae CcrZ is 264 amino acids long and is predicted to have a single APH (aminoglycoside phosphotransferase enzyme family) domain (Fig. 5D). Sequence alignment using Psi-BLAST showed homology with phosphotransferase enzyme family proteins, while pairwise comparisons of profile-hidden Markov models (HMMs) using HHpred (*51*) identified homologies with ethanolamine- and choline kinases. Despite various attempts, we have not been able to establish any biochemical activity or nucleotide binding for recombinant purified CcrZ and were unable to produce protein crystals, probably because of its rapid precipitation in solution. Nevertheless, as CcrZ is highly conserved in Firmicutes, we aligned CcrZ protein sequence with 1000 protein sequences from UniRef50 and identified three residues conserved in more than 95% of the proteins (D159, N164 and D177) and two other residues (H157 and D189) in more than 80% (Fig. 5D and fig. S4D). To determine the position of these residues, the *S. pneumoniae* CcrZ protein sequence was mapped onto the crystal structure of the best hit from the HMM alignment, the choline kinase LicA, in complex with adenosine monophosphate (AMP) (pdb 4R78). Interestingly, these five conserved residues appear to be in spatial proximity to AMP and thus to a putative nucleotide-binding pocket (Fig. 5E). Comparison of CcrZ and LicA sequences shows a conserved Brenner's motif [HXDhX3N] (residues CcrZ H157 – N164) found in most phosphotransferases (Fig. 5D). In this motif, LicA-N187 (CcrZ-N164) was shown to interact with the α-phosphate moiety of AMP (*52*) and LicA-D176 (CcrZ-D159) was shown to be crucial for hydrogen bond formation with the hydroxyl moiety of choline. Furthermore, it also has a conserved motif found in phosphotranspherases (APH), in which LicA-D194 (CcrZ-D177) was

shown to interact with the α-phosphate moiety of AMP. CcrZ-D189 corresponds to residue D313 of the choline kinase A (cka-2) of *Caenorhabditis elegans*, a residue which was proposed to stabilize the cka-2 dimer as well as the catalytic site (*53*). CcrZ however does not possess the conserved hydrophobic residues specific to choline- and ethanolamine-kinases necessary for choline binding, but instead has several polar amino acids at these positions (*e.g.,* the crucial residues LicA-Y197 and V178 corresponding to CcrZ-S180 and R161). Mutational analysis of the five conserved residues of CcrZ showed that at least H157, N164 and D177 are essential for CcrZ's function in *S. pneumoniae* (Fig. 5F), while mutating CcrZ-D159 or CcrZ-D189 did not lead to any growth defect. All three essential mutants were properly produced (fig. S1C) and CcrZ-H157A and CcrZ-D177A could still localize at the septum (Fig. 5G). Therefore, these three residues are crucial for the function of CcrZ. It is interesting to note that none of the three mutants was dominant negative when expressed together with a wild type CcrZ. Given the high similarity with LicA, it is very likely that CcrZ can bind an as of yet unknown nucleotide.

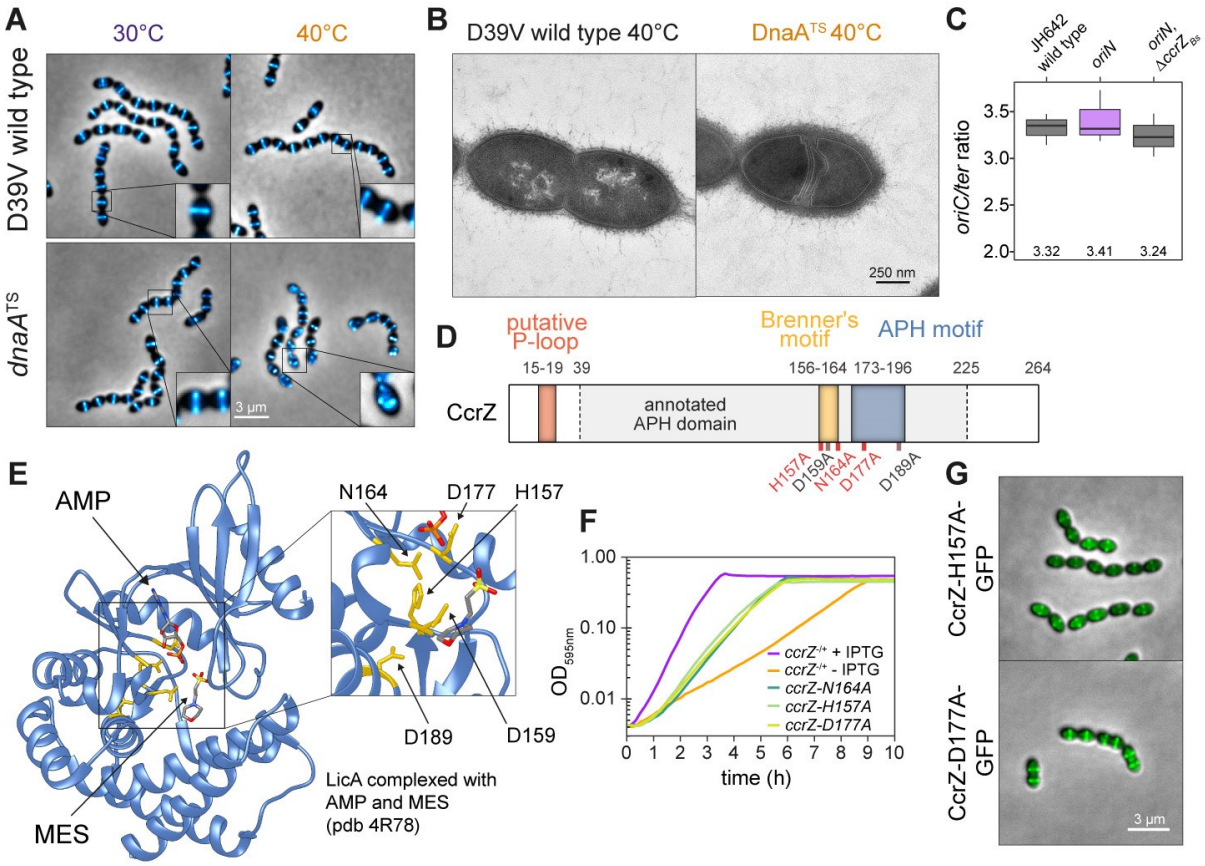

Fig. 5. CcrZ activates DnaA-dependent replication initiation

(**A**) Localization of FtsZ-mTurquoise2 in a thermo-sensitive DnaA strain (*dnaA*^{TS}) at permissive (30°C) and non-permissive (40°C) temperatures shows that *dnaA* inactivation leads to a similar phenotype as *ccrZ* inactivation. (**B**), TEM of DnaA^{TS} at non-permissive temperature (40°C) indicates the presence of multiple septa, similarly to a Δ*ccrZ* mutant. (**C**) When replication is driven in a RepN-dependent manner in *B. subtilis* (*oriN*), no decrease in *ori/ter* ratio can be observed in absence of $ccrZ_{Bs}$ (*oriN,* Δ$ccrZ_{Bs}$). (**D**) Schematic representation of CcrZ motifs. CcrZ has one putative domain annotated APH (Phosphotransferase enzyme family; PFAM01636). Sequence alignment with several kinases revealed the presence of a conserved P-loop, APH and Brenner's motifs, found in most phosphotransferases. Locations of mutations made for 3 essential (red) and 2 non-essential (black) conserved residues are shown underneath. (**E**) LicA choline kinase structure complexed with AMP and MES (2-(N-morpholino)ethanesulfonic acid). The 5 residues indicated in yellow are conserved between CcrZ and LicA (and highly conserved within Firmicutes). (**F**) Mutation of three of these five conserved residues in the putative ATP binding pocket leads to growth defects. (**G**) Localization of CcrZ- H157A-GFP and CcrZ-D177A-GFP is not impaired.

A model for CcrZ-controlled DNA replication in *S. pneumoniae*

We showed above that CcrZ is fundamental for DnaA-dependent DNA replication initiation in *B. subtilis* and that *S. pneumoniae* CcrZ localizes at mid-cell for most of the cell cycle. In *S. pneumoniae*, once DNA replication initiates at mid-cell, the origins localize at both future division sites, while the replication machinery stays near the Z-ring until completion of replication and closure of the septum (*35*). We therefore hypothesized that CcrZ is brought to mid-cell by FtsZ to promote initiation of DNA replication. To map the hierarchy of events that take place during the pneumococcal cell cycle, we constructed a triple-labeled strain (strain *ccrZ-mKate2 dnaN-sfTQ*^{OX} *parB*$_p$*-mYFP*) in which CcrZ is fused to a red fluorescent protein, DNA replication is visualized by a DnaN fusion to a cyan fluorescent protein, and the origin of replication is marked with a yellow fluorescent reporter (see Methods). Imaging of this strain by short time-lapse fluorescence microscopy (< 1 min) revealed that DNA replication initiates once CcrZ is assembled at mid-cell, rapidly followed by segregation of the newly replicated origins as cells elongate (Fig. 6, A, B C and D and Movie S8). The replication machinery remains near the old division site together with CcrZ, only to move to the new cell division sites once DNA replication is complete. This data supports a model in which FtsZ brings CcrZ to *oriC* to stimulate DnaA to fire a new round of replication ensuring that DNA replication only commences after the origins are well segregated and positioned at the new mid-cell position. Indeed, DnaA co-localizes with CcrZ in new-born cells (fig. S5). In the absence of CcrZ, initiation of DNA replication is mis-timed and occurs too late relative to cellular growth and Z-ring formation, frequently leading to futile division events, mis-segregated chromosomes and anucleate cells (Fig. 6E).

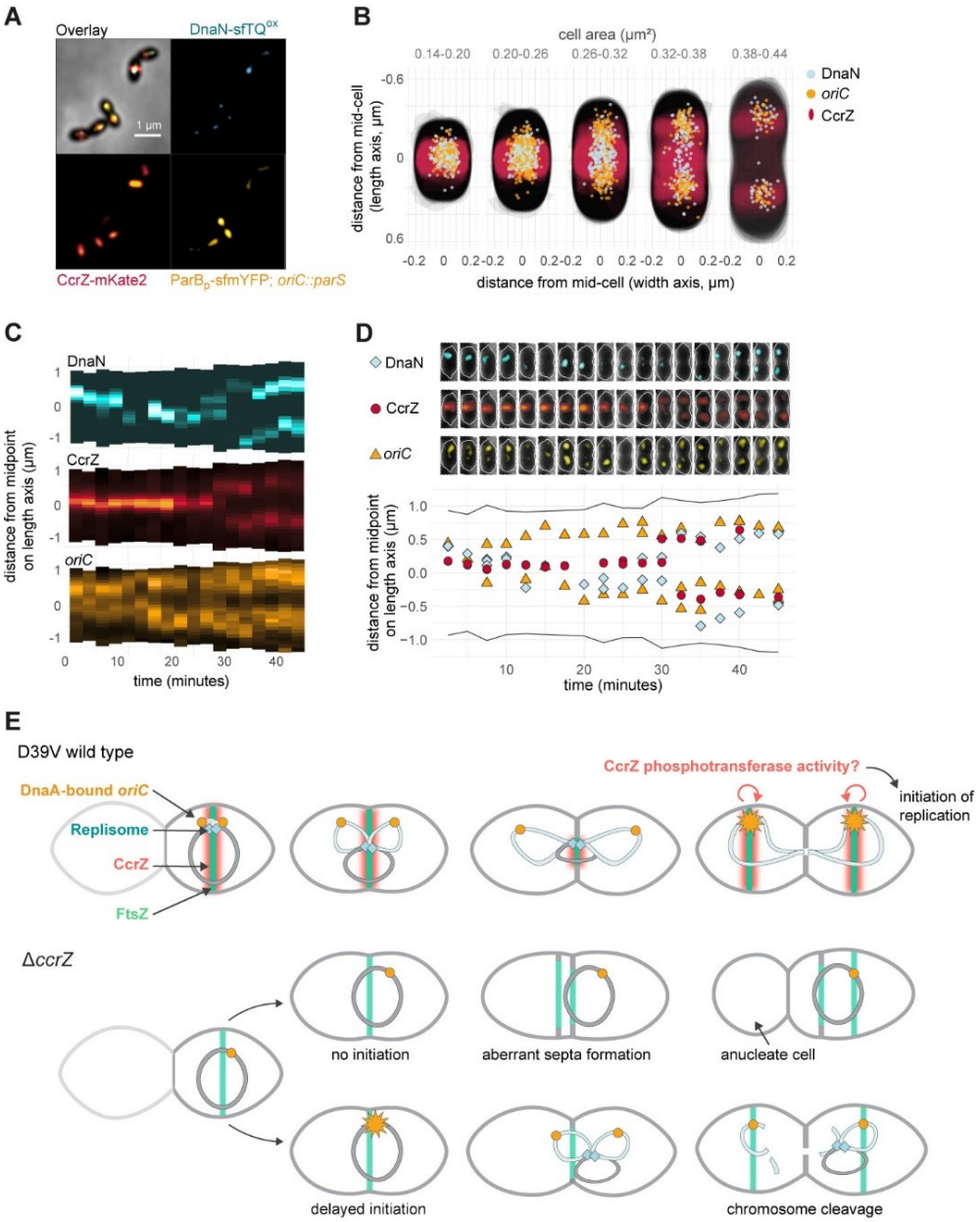

Fig. 6. Spatio-temporal localization of CcrZ via FtsZ ensures proper timing of DNA replication in *S. pneumoniae*

(**A**) Microscopy of the origin of replication (yellow), replication fork (cyan) and CcrZ (red) in live *S. pneumoniae* wild type background cells. (**B**) DnaN, *oriC* and CcrZ localizations grouped by cell area (µm^2) in five equally sized groups. Analyzed from snapshots of exponentially growing cells. (**C**) Single-cell kymographs of DnaN, CcrZ and *oriC* localizations in a 2:30 minute interval time-lapse movie. (**D**) Tracked DnaN, *oriC* and CcrZ over time in a single cell. Top: overlay of fluorescence, cell outline and phase-contrast of the cell displayed in panel c and bottom: fluorescence localization on the length axis of the same single cell over time. (**E**) Model for spatio-temporal control of replication by CcrZ. In *S. pneumoniae*, CcrZ is brought to the middle of the cell where the DnaA-bound origin of replication is already positioned. CcrZ then stimulates DnaA to trigger DNA replication by an as of yet unknown activity, possibly involving a phosphor-transfer event. While the precise regulation and localization of CcrZ seems diverse between different organisms, CcrZ's activity to stimulate DNA replication is conserved, at least in *S. pneumoniae, S. aureus* and *B. subtilis.*

Conclusions

The principal contribution of this work is the identification and initial functional characterization of a new mechanism for cell cycle regulation in *S. pneumoniae* via the CcrZ protein. We show that CcrZ's septal localization occurs via a direct interaction with the C-terminus of FtsZ. Our data is consistent with a model in which, once positioned at mid-cell where the DnaA-bound origin of replication is located, CcrZ stimulates DnaA, likely by phosphorylation of an intermediate molecule, to initiate DNA replication (Fig. 6). Importantly, CcrZ's function of controlling DnaA seems conserved in *S. aureus* and *B. subtilis*, and likely in many other Gram-positive bacteria (fig. S1A).

Besides the production of anucleate cells and cells with cleaved chromosomes, *ccrZ* mutants contain multiple aberrant division septa (Fig. 6E). Notably, this is phenocopied by a temperature sensitive DnaA allele. This indicates that chromosome replication itself, and correct localization of the chromosome has an important role in nucleoid occlusion: when initiation is too late and the new daughter chromosomes are not fully segregated, division can take place over the DNA resulting in dissected chromosomes. We also observed multiple division septa in cells depleted for CcrZ that are likely caused by mis-timed chromosome segregation whereby Z-rings are formed adjacent to the nucleoid. These phenotypes are reminiscent of observations made for *E. coli* and *B. subtilis* that showed that after arrest of DNA replication, many cells continued to elongate without dividing, but FtsZ rings continued to form and almost always were located to the side of nucleoids (*54*, *55*). In this respect, it is interesting to note that the *S. aureus* Noc system also controls DNA replication, as Δ*noc* cells over-initiate DNA replication (*56*). In support of our findings, a lethal Δ*noc* Δ*comEB* double mutant in *S. aureus* could be rescued by a suppressor mutation in $ccrZ_{Sa}$ (*56*), further indicating that $CcrZ_{Sa}$ is also involved in the control of DNA replication in *S. aureus.*

This work uncovers a novel mechanism in which a single protein links cell division with DNA replication control. In this model, Z-ring formation is used as a timer for the initiation of DNA replication. When cell division terminates, leading to the formation of another Z-ring at the new division site, CcrZ is brought along and can activate a new round of DNA replication. This simple system ensures that DNA replication only commences a single time per cell cycle in newborn cells. It will be interesting to see how CcrZ controls the cell cycle in other bacteria, what the involved biochemical activities are and whether CcrZ will prove as a new target for innovative antibiotics.

References and Notes:

1. H. Harashima, N. Dissmeyer, A. Schnittger, Cell cycle control across the eukaryotic kingdom. *Trends Cell Biol.* **23**, 345–356 (2013).
2. E. Boye, K. Nordström, Coupling the cell cycle to cell growth. *EMBO Rep.* **4**, 757–60 (2003).
3. R. Reyes-Lamothe, D. J. Sherratt, The bacterial cell cycle, chromosome inheritance and cell growth. *Nat. Rev. Microbiol.*, 1 (2019).
4. N. O. Kjeldgaard, O. MaalOe, M. Schaechter, The Transition Between Different Physiological States During Balanced Growth of Salmonella typhimurium. *J. Gen. Microbiol.* **19**, 607–616 (1958).
5. M. Schaechter, O. MaalOe, N. O. Kjeldgaard, Dependency on Medium and Temperature of Cell Size and Chemical Composition during Balanced Growth of Salmonella typhimurium. *J. Gen. Microbiol.* **19**, 592–606 (1958).
6. W. D. Donachie, Relationship between cell size and time of initiation of DNA replication. *Nature*. **219**, 1077–9 (1968).
7. S. Cooper, C. E. Helmstetter, Chromosome replication and the division cycle of Escherichia coli Br. *J. Mol. Biol.* **31**, 519–540 (1968).
8. M. Campos, I. V. Surovtsev, S. Kato, A. Paintdakhi, B. Beltran, S. E. Ebmeier, C. Jacobs-Wagner, A Constant Size Extension Drives Bacterial Cell Size Homeostasis. *Cell*. **159**, 1433–1446 (2014).
9. S. Taheri-Araghi, S. Bradde, J. T. Sauls, N. S. Hill, P. A. Levin, J. Paulsson, M. Vergassola, S. Jun, Cell-size control and homeostasis in bacteria. *Curr. Biol.* **25**, 385–391 (2015).
10. S. Wold, K. Skarstad, H. B. Steen, T. Stokke, E. Boye, The initiation mass for DNA replication in Escherichia coli K-12 is dependent on growth rate. *EMBO J.* **13**, 2097–102 (1994).
11. F. Si, G. Le Treut, J. T. Sauls, S. Vadia, P. A. Levin, S. Jun, Mechanistic Origin of Cell-Size Control and Homeostasis in Bacteria. *Curr. Biol.* **29**, 1760-1770.e7 (2019).
12. M. Wallden, D. Fange, E. G. Lundius, Ö. Baltekin, J. Elf, The Synchronization of Replication and Division Cycles in Individual E. coli Cells. *Cell*. **166**, 729–739 (2016).
13. N. E. Kleckner, K. Chatzi, M. A. White, J. K. Fisher, M. Stouf, Coordination of Growth, Chromosome Replication/Segregation, and Cell Division in E. coli. *Front. Microbiol.* **9**, 1469 (2018).
14. N. Kleckner, J. K. Fisher, M. Stouf, M. A. White, D. Bates, G. Witz, The bacterial nucleoid: nature, dynamics and sister segregation. *Curr. Opin. Microbiol.* **22**, 127–37 (2014).
15. I. V. Hajduk, C. D. A. Rodrigues, E. J. Harry, Connecting the dots of the bacterial cell cycle: Coordinating chromosome replication and segregation with cell division. *Semin. Cell Dev. Biol.* **53**, 2–9 (2016).
16. O. Espéli, R. Borne, P. Dupaigne, A. Thiel, E. Gigant, R. Mercier, F. Boccard, A MatP-divisome interaction coordinates chromosome segregation with cell division in E. coli. *EMBO J.* **31**, 3198–211 (2012).

17. H. Zheng, P.-Y. Ho, M. Jiang, B. Tang, W. Liu, D. Li, X. Yu, N. E. Kleckner, A. Amir, C. Liu, Interrogating the Escherichia coli cell cycle by cell dimension perturbations. *Proc. Natl. Acad. Sci. U. S. A.* **113**, 15000–15005 (2016).

18. P. G. Huls, N. O. E. Vischer, C. L. Woldringh, Different Amounts of DNA in Newborn Cells of Escherichia coli Preclude a Role for the Chromosome in Size Control According to the "Adder" Model. *Front. Microbiol.* **9**, 664 (2018).

19. T. Katayama, (Springer, Singapore, 2017; http://link.springer.com/10.1007/978-981-10-6955-0_4), pp. 79–98.

20. T. Katayama, K. Kasho, H. Kawakami, The DnaA Cycle in Escherichia coli: Activation, Function and Inactivation of the Initiator Protein. *Front. Microbiol.* **8**, 2496 (2017).

21. A. Løbner-Olesen, K. Skarstad, F. G. Hansen, K. von Meyenburg, E. Boye, The DnaA protein determines the initiation mass of Escherichia coli K-12. *Cell*. **57**, 881–889 (1989).

22. O. Pierucci, M. Rickert, C. E. Helmstetter, DnaA protein overproduction abolishes cell cycle specificity of DNA replication from oriC in Escherichia coli. *J. Bacteriol.* **171**, 3760–6 (1989).

23. I. Flåtten, S. Fossum-Raunehaug, R. Taipale, S. Martinsen, K. Skarstad, The DnaA Protein Is Not the Limiting Factor for Initiation of Replication in Escherichia coli. *PLOS Genet.* **11**, e1005276 (2015).

24. N. S. Hill, R. Kadoya, D. K. Chattoraj, P. A. Levin, Cell Size and the Initiation of DNA Replication in Bacteria. *PLoS Genet.* **8**, e1002549 (2012).

25. H. Murray, A. Koh, Multiple Regulatory Systems Coordinate DNA Replication with Cell Growth in Bacillus subtilis. *PLoS Genet.* **10**, e1004731 (2014).

26. P. Bisicchia, S. Arumugam, P. Schwille, D. Sherratt, MinC, MinD, and MinE drive counter-oscillation of early-cell-division proteins prior to Escherichia coli septum formation. *MBio*. **4**, e00856-13 (2013).

27. A. L. Marston, H. B. Thomaides, D. H. Edwards, M. E. Sharpe, J. Errington, Polar localization of the MinD protein of Bacillus subtilis and its role in selection of the mid-cell division site. *Genes Dev.* **12**, 3419–30 (1998).

28. L. J. Wu, J. Errington, Nucleoid occlusion and bacterial cell division. *Nat. Rev. Microbiol.* **10**, 8–12 (2012).

29. M. G. Pinho, M. Kjos, J.-W. Veening, How to get (a)round: mechanisms controlling growth and division of coccoid bacteria. *Nat. Rev. Microbiol.* **11**, 601–614 (2013).

30. A. D. Land, H.-C. T. Tsui, O. Kocaoglu, S. A. Vella, S. L. Shaw, S. K. Keen, L.-T. Sham, E. E. Carlson, M. E. Winkler, Requirement of essential Pbp2x and GpsB for septal ring closure in Streptococcus pneumoniae D39. *Mol. Microbiol.* **90**, 939–955 (2013).

31. C. Mercy, A. Ducret, J. Slager, J.-P. Lavergne, C. Freton, S. N. Nagarajan, P. S. Garcia, M.-F. Noirot-Gros, N. Dubarry, J. Nourikyan, J.-W. Veening, C. Grangeasse, RocS drives chromosome segregation and nucleoid protection in Streptococcus pneumoniae. *Nat. Microbiol.*, 1 (2019).

32. A. Fleurie, C. Lesterlin, S. Manuse, C. Zhao, C. Cluzel, J.-P. Lavergne, M. Franz-Wachtel,

B. Macek, C. Combet, E. Kuru, M. S. VanNieuwenhze, Y. V. Brun, D. Sherratt, C. Grangeasse, MapZ marks the division sites and positions FtsZ rings in Streptococcus pneumoniae. *Nature*. **516**, 259–262 (2014).

33. N. Holečková, L. Doubravová, O. Massidda, V. Molle, K. Buriánková, O. Benada, O. Kofroňová, A. Ulrych, P. Branny, LocZ is a new cell division protein involved in proper septum placement in Streptococcus pneumoniae. *MBio*. **6**, e01700-14 (2014).

34. A. J. Perez, Y. Cesbron, S. L. Shaw, J. B. Villicana, H.-C. T. Tsui, M. J. Boersma, Z. A. Ye, Y. Tovpeko, C. Dekker, S. Holden, M. E. Winkler, Movement dynamics of divisome proteins and PBP2x:FtsW in cells of Streptococcus pneumoniae. *Proc. Natl. Acad. Sci.* **116**, 3211–3220 (2019).

35. R. van Raaphorst, M. Kjos, J.-W. Veening, Chromosome segregation drives division site selection inStreptococcus pneumoniae. *Proc. Natl. Acad. Sci. U. S. A.* **114**, E5959–E5968 (2017).

36. X. Liu, C. Gallay, M. Kjos, A. Domenech, J. Slager, S. P. van Kessel, K. Knoops, R. A. Sorg, J.-R. Zhang, J.-W. Veening, High-throughput CRISPRi phenotyping identifies new essential genes inStreptococcus pneumoniae. *Mol. Syst. Biol.* **13**, 931 (2017).

37. J. Nourikyan, M. Kjos, C. Mercy, C. Cluzel, C. Morlot, M.-F. Noirot-Gros, S. Guiral, J.-P. Lavergne, J.-W. Veening, C. Grangeasse, Autophosphorylation of the Bacterial Tyrosine-Kinase CpsD Connects Capsule Synthesis with the Cell Cycle in Streptococcus pneumoniae. *PLOS Genet.* **11**, e1005518 (2015).

38. S. Du, J. Lutkenhaus, Assembly and activation of the *Escherichia coli* divisome. *Mol. Microbiol.* **105**, 177–187 (2017).

39. A. Krogh, B. Larsson, G. von Heijne, E. L. . Sonnhammer, Predicting transmembrane protein topology with a hidden markov model: application to complete genomes. *J. Mol. Biol.* **305**, 567–580 (2001).

40. A. M. Oliveira Paiva, A. H. Friggen, L. Qin, R. Douwes, R. T. Dame, W. K. Smits, The Bacterial Chromatin Protein HupA Can Remodel DNA and Associates with the Nucleoid in Clostridium difficile. *J. Mol. Biol.* **431**, 653–672 (2019).

41. C. R. Bodle, M. P. Hayes, J. B. O'Brien, D. L. Roman, Development of a bimolecular luminescence complementation assay for RGS: G protein interactions in cells. *Anal. Biochem.* **522**, 10–17 (2017).

42. G. Karimova, J. Pidoux, A. Ullmann, D. Ladant, A bacterial two-hybrid system based on a reconstituted signal transduction pathway. *Proc. Natl. Acad. Sci. U. S. A.* **95**, 5752–6 (1998).

43. S. Pichoff, J. Lutkenhaus, Identification of a region of FtsA required for interaction with FtsZ. *Mol. Microbiol.* **64**, 1129–1138 (2007).

44. M. Kjos, R. Aprianto, V. E. Fernandes, P. W. Andrew, J. A. G. van Strijp, R. Nijland, J.-W. Veening, Bright fluorescent Streptococcus pneumoniae for live-cell imaging of host-pathogen interactions. *J. Bacteriol.* **197**, 807–18 (2015).

45. L. Felicori, K. H. Jameson, P. Roblin, M. J. Fogg, T. Garcia-Garcia, M. Ventroux, M. V. Cherrier, A. Bazin, P. Noirot, A. J. Wilkinson, F. Molina, L. Terradot, M.-F. Noirot-Gros, Tetramerization and interdomain flexibility of the replication initiation controller YabA

enables simultaneous binding to multiple partners. *Nucleic Acids Res.* **44**, 449–463 (2016).

46. J. Slager, M. Kjos, L. Attaiech, J.-W. Veening, Antibiotic-Induced Replication Stress Triggers Bacterial Competence by Increasing Gene Dosage near the Origin. *Cell*. **157**, 395–406 (2014).

47. K. E. Duderstadt, K. Chuang, J. M. Berger, DNA stretching by bacterial initiators promotes replication origin opening. *Nature*. **478**, 209–213 (2011).

48. G. Scholefield, J. Errington, H. Murray, Soj/ParA stalls DNA replication by inhibiting helix formation of the initiator protein DnaA. *EMBO J.* **31**, 1542–55 (2012).

49. X. Liu, J. M. Kimmey, L. Matarazzo, V. de Bakker, L. Van Maele, J. C. Sirard, V. Nizet, J. W. Veening, Exploration of Bacterial Bottlenecks and Streptococcus pneumoniae Pathogenesis by CRISPRi-Seq. *Cell Host Microbe* (2020), doi:10.1016/j.chom.2020.10.001.

50. S. Bigot, V. Sivanathan, C. Possoz, F. X. Barre, F. Cornet, FtsK, a literate chromosome segregation machine. *Mol. Microbiol.* **64** (2007), pp. 1434–1441.

51. J. Soding, A. Biegert, A. N. Lupas, The HHpred interactive server for protein homology detection and structure prediction. *Nucleic Acids Res.* **33**, W244–W248 (2005).

52. L. Wang, Y.-L. Jiang, J.-R. Zhang, C.-Z. Zhou, Y. Chen, Structural and Enzymatic Characterization of the Choline Kinase LicA from Streptococcus pneumoniae. *PLoS One*. **10**, e0120467 (2015).

53. S. BRENNER, Phosphotransferase sequence homology. *Nature*. **329**, 21–21 (1987).

54. X. C. Yu, W. Margolin, FtsZ ring clusters in min and partition mutants: Role of both the Min system and the nucleoid in regulating FtsZ ring localization. *Mol. Microbiol.* **32**, 315–326 (1999).

55. E. J. Harry, J. Rodwell, R. G. Wake, Co-ordinating DNA replication with cell division in bacteria: a link between the early stages of a round of replication and mid-cell Z ring assembly. *Mol. Microbiol.* **33**, 33–40 (1999).

56. T. Pang, X. Wang, H. C. Lim, T. G. Bernhardt, D. Z. Rudner, The nucleoid occlusion factor Noc controls DNA replication initiation in Staphylococcus aureus. *PLoS Genet.* **13**, e1006908 (2017).

57. J. Slager, R. Aprianto, J.-W. Veening, Deep genome annotation of the opportunistic human pathogen Streptococcus pneumoniae D39. *Nucleic Acids Res.* **46**, 9971–9989 (2018).

58. A. Domenech, J. Slager, J.-W. Veening, Antibiotic-Induced Cell Chaining Triggers Pneumococcal Competence by Reshaping Quorum Sensing to Autocrine-Like Signaling. *Cell Rep.* **25**, 2390-2400.e3 (2018).

59. I. R. Monk, J. J. Tree, B. P. Howden, T. P. Stinear, T. J. Foster, Complete Bypass of Restriction Systems for Major Staphylococcus aureus Lineages. *MBio*. **6**, e00308-15 (2015).

60. J. Löfblom, N. Kronqvist, M. Uhlén, S. Ståhl, H. Wernérus, Optimization of electroporation-mediated transformation: Staphylococcus carnosus as model organism. *J. Appl. Microbiol.* **102**, 736–747 (2007).

61. K. J. Jaacks, J. Healy, R. Losick, A. D. Grossman, Identification and characterization of genes controlled by the sporulation-regulatory gene spo0H in Bacillus subtilis. *J. Bacteriol.* **171**, 4121–4129 (1989).

62. M. Perego, G. B. Spiegelman, J. A. Hoch, Structure of the gene for the transition state regulator, abrB: regulator synthesis is controlled by the spo0A sporulation gene in Bacillus subtilis. *Mol. Microbiol.* **2**, 689–699 (1988).

63. L. E. Keller, A.-S. Rueff, J. Kurushima, J.-W. Veening, L. E. Keller, A.-S. Rueff, J. Kurushima, J.-W. Veening, Three New Integration Vectors and Fluorescent Proteins for Use in the Opportunistic Human Pathogen Streptococcus pneumoniae. *Genes (Basel).* **10**, 394 (2019).

64. D. G. Gibson, L. Young, R.-Y. Chuang, J. C. Venter, C. A. Hutchison, H. O. Smith, Enzymatic assembly of DNA molecules up to several hundred kilobases. *Nat. Methods*. **6**, 343–345 (2009).

65. R. A. Sorg, O. P. Kuipers, J.-W. Veening, Gene Expression Platform for Synthetic Biology in the Human Pathogen *Streptococcus pneumoniae*. *ACS Synth. Biol.* **4**, 228–239 (2015).

66. C. Engler, R. Kandzia, S. Marillonnet, A one pot, one step, precision cloning method with high throughput capability. *PLoS One*. **3**, e3647 (2008).

67. J. Hoskins, W. E. Alborn, J. Arnold, L. C. Blaszczak, S. Burgett, B. S. DeHoff, S. T. Estrem, L. Fritz, D. J. Fu, W. Fuller, C. Geringer, R. Gilmour, J. S. Glass, H. Khoja, A. R. Kraft, R. E. Lagace, D. J. LeBlanc, L. N. Lee, E. J. Lefkowitz, J. Lu, P. Matsushima, S. M. McAhren, M. McHenney, K. McLeaster, C. W. Mundy, T. I. Nicas, F. H. Norris, M. O'Gara, R. B. Peery, G. T. Robertson, P. Rockey, P. M. Sun, M. E. Winkler, Y. Yang, M. Young-Bellido, G. Zhao, C. A. Zook, R. H. Baltz, S. R. Jaskunas, P. R. Rosteck, P. L. Skatrud, J. I. Glass, Genome of the bacterium Streptococcus pneumoniae strain R6. *J. Bacteriol.* **183**, 5709–17 (2001).

68. H. Tettelin, K. E. Nelson, I. T. Paulsen, J. A. Eisen, T. D. Read, S. Peterson, J. Heidelberg, R. T. DeBoy, D. H. Haft, R. J. Dodson, A. S. Durkin, M. Gwinn, J. F. Kolonay, W. C. Nelson, J. D. Peterson, L. A. Umayam, O. White, S. L. Salzberg, M. R. Lewis, D. Radune, E. Holtzapple, H. Khouri, A. M. Wolf, T. R. Utterback, C. L. Hansen, L. A. McDonald, T. V Feldblyum, S. Angiuoli, T. Dickinson, E. K. Hickey, I. E. Holt, B. J. Loftus, F. Yang, H. O. Smith, J. C. Venter, B. A. Dougherty, D. A. Morrison, S. K. Hollingshead, C. M. Fraser, Complete genome sequence of a virulent isolate of Streptococcus pneumoniae. *Science*. **293**, 498–506 (2001).

69. R. A. Sorg, L. Lin, G. S. van Doorn, M. Sorg, J. Olson, V. Nizet, J.-W. Veening, Collective Resistance in Microbial Communities by Intracellular Antibiotic Deactivation. *PLOS Biol.* **14**, e2000631 (2016).

70. P. O'Neil, S. Lovell, N. Mehzabeen, K. Battaile, I. Biswas, Crystal structure of histone-like protein from Streptococcus mutans refined to 1.9 Å resolution. *Acta Crystallogr. Sect. F, Struct. Biol. Commun.* **72**, 257–62 (2016).

71. G. A. Stamsås, I. S. Myrbråten, D. Straume, Z. Salehian, J.-W. Veening, L. S. Håvarstein, M. Kjos, CozEa and CozEb play overlapping and essential roles in controlling cell division in *Staphylococcus aureus*. *Mol. Microbiol.* **109**, 615–632 (2018).

72. M.-L. Diebold-Durand, F. Bürmann, S. Gruber, (Humana, New York, NY, 2019; http://link.springer.com/10.1007/978-1-4939-9520-2_5), pp. 49–61.

73. P. Youngman, H. Poth, B. Green, K. York, G. Olmedo, G. Olmeda, K. Wager-Smith, Methods for genetic manipulation, cloning and functional analysis of sporulation genes in Bacillus subtilis (1989), (available at https://www.scienceopen.com/document?vid=613e83fa-7742-44f9-94b5-97273cb0168a).

74. A. K. Hassan, S. Moriya, M. Ogura, T. Tanaka, F. Kawamura, N. Ogasawara, Suppression of initiation defects of chromosome replication in Bacillus subtilis dnaA and oriC-deleted mutants by integration of a plasmid replicon into the chromosomes. *J. Bacteriol.* **179**, 2494–502 (1997).

75. D. G. Yansura, D. J. Henner, Use of the Escherichia coli lac repressor and operator to control gene expression in Bacillus subtilis. *Proc. Natl. Acad. Sci. U. S. A.* **81**, 439–43 (1984).

76. K. P. Lemon, I. Kurtser, A. D. Grossman, Effects of replication termination mutants on chromosome partitioning in Bacillus subtilis. *Proc. Natl. Acad. Sci. U. S. A.* **98**, 212–7 (2001).

77. I. G. de Jong, K. Beilharz, O. P. Kuipers, J.-W. Veening, Live Cell Imaging of Bacillus subtilis and Streptococcus pneumoniae using Automated Time-lapse Microscopy. *J. Vis. Exp.* (2011), doi:10.3791/3145.

78. A. Paintdakhi, B. Parry, M. Campos, I. Irnov, J. Elf, I. Surovtsev, C. Jacobs-Wagner, Oufti: an integrated software package for high-accuracy, high-throughput quantitative microscopy analysis. *Mol. Microbiol.* **99**, 767–777 (2016).

79. T. Ursell, T. K. Lee, D. Shiomi, H. Shi, C. Tropini, R. D. Monds, A. Colavin, G. Billings, I. Bhaya-Grossman, M. Broxton, B. E. Huang, H. Niki, K. C. Huang, Rapid, precise quantification of bacterial cellular dimensions across a genomic-scale knockout library. *BMC Biol.* **15**, 17 (2017).

80. A. Ducret, E. M. Quardokus, Y. V Brun, MicrobeJ, a tool for high throughput bacterial cell detection and quantitative analysis. *Nat. Microbiol.* **1**, 16077 (2016).

81. V. E. A. Caldas, C. M. Punter, H. Ghodke, A. Robinson, A. M. van Oijen, iSBatch: a batch-processing platform for data analysis and exploration of live-cell single-molecule microscopy images and other hierarchical datasets. *Mol. Biosyst.* **11**, 2699–2708 (2015).

82. R. van Raaphorst, M. Kjos, J.-W. Veening, BactMAP: an R package for integrating, analyzing and visualizing bacterial microscopy data. *bioRxiv*, 728782 (2019).

83. F. W. Studier, Protein production by auto-induction in high density shaking cultures. *Protein Expr. Purif.* **41**, 207–34 (2005).

84. M. H. Kubala, O. Kovtun, K. Alexandrov, B. M. Collins, Structural and thermodynamic analysis of the GFP:GFP-nanobody complex. *Protein Sci.* **19**, 2389–401 (2010).

85. N. A. Kulak, G. Pichler, I. Paron, N. Nagaraj, M. Mann, Minimal, encapsulated proteomic-sample processing applied to copy-number estimation in eukaryotic cells. *Nat. Methods*. **11**, 319–324 (2014).

86. *,† Andrew Keller, *,† Alexey I. Nesvizhskii, and Eugene Kolker, R. Aebersold,

Empirical Statistical Model To Estimate the Accuracy of Peptide Identifications Made by MS/MS and Database Search (2002), doi:10.1021/AC025747H.

87. *,† Alexey I. Nesvizhskii, *,† Andrew Keller, ‡ and Eugene Kolker, R. Aebersold, A Statistical Model for Identifying Proteins by Tandem Mass Spectrometry (2003), doi:10.1021/AC0341261.

88. S. P. Ouellette, K. J. Rueden, E. Gauliard, L. Persons, P. A. de Boer, D. Ladant, Analysis of MreB interactors in Chlamydia reveals a RodZ homolog but fails to detect an interaction with MraY. *Front. Microbiol.* **5**, 279 (2014).

89. D. E. Deatherage, J. E. Barrick, Identification of mutations in laboratory-evolved microbes from next-generation sequencing data using breseq. *Methods Mol. Biol.* **1151**, 165–88 (2014).

90. D. Szklarczyk, A. L. Gable, D. Lyon, A. Junge, S. Wyder, J. Huerta-Cepas, M. Simonovic, N. T. Doncheva, J. H. Morris, P. Bork, L. J. Jensen, C. von Mering, STRING v11: protein-protein association networks with increased coverage, supporting functional discovery in genome-wide experimental datasets. *Nucleic Acids Res.* **47**, D607–D613 (2019).

91. L. Zimmermann, A. Stephens, S.-Z. Nam, D. Rau, J. Kübler, M. Lozajic, F. Gabler, J. Söding, A. N. Lupas, V. Alva, A Completely Reimplemented MPI Bioinformatics Toolkit with a New HHpred Server at its Core. *J. Mol. Biol.* **430**, 2237–2243 (2018).

92. O. T. Avery, C. M. Macleod, M. McCarty, STUDIES ON THE CHEMICAL NATURE OF THE SUBSTANCE INDUCING TRANSFORMATION OF PNEUMOCOCCAL TYPES : INDUCTION OF TRANSFORMATION BY A DESOXYRIBONUCLEIC ACID FRACTION ISOLATED FROM PNEUMOCOCCUS TYPE III. *J. Exp. Med.* **79**, 137–58 (1944).

93. H. Tettelin, K. E. Nelson, I. T. Paulsen, J. A. Eisen, T. D. Read, S. Peterson, J. Heidelberg, R. T. DeBoy, D. H. Haft, R. J. Dodson, A. S. Durkin, M. Gwinn, J. F. Kolonay, W. C. Nelson, J. D. Peterson, L. A. Umayam, O. White, S. L. Salzberg, M. R. Lewis, D. Radune, E. Holtzapple, H. Khouri, A. M. Wolf, T. R. Utterback, C. L. Hansen, L. A. McDonald, T. V. Feldblyum, S. Angiuoli, T. Dickinson, E. K. Hickey, I. E. Holt, B. J. Loftus, F. Yang, H. O. Smith, J. C. Venter, B. A. Dougherty, D. A. Morrison, S. K. Hollingshead, C. M. Fraser, Complete genome sequence of a virulent isolate of Streptococcus pneumoniae. *Science (80-.).* **293**, 498–506 (2001).

94. M. J. Horsburgh, J. L. Aish, I. J. White, L. Shaw, J. K. Lithgow, S. J. Foster, sigmaB modulates virulence determinant expression and stress resistance: characterization of a functional rsbU strain derived from Staphylococcus aureus 8325-4. *J. Bacteriol.* **184**, 5457–67 (2002).

95. A. K. Hassan, S. Moriya, M. Ogura, T. Tanaka, F. Kawamura, N. Ogasawara, Suppression of initiation defects of chromosome replication in Bacillus subtilis dnaA and oriC-deleted mutants by integration of a plasmid replicon into the chromosomes. *J. Bacteriol.* **179**, 2494–502 (1997).

Acknowledgments: We appreciate the assistance from the Electron Microscopy Facility (EMF) and the Protein Analysis Facility (PAF) at the University of Lausanne (UNIL) and thank them for their support. We thank Wiep Klaas Smits (LUMC) for the Split-luc sequences and Tanneke den Blaauwen (UVA) for the mTQ^{ox} sequence prior to publication, Arnau Domenech (UNIL) for construction of strain *hlpA-LgBit hlpA-SmBit* and Zhian Salehian (NMBU) for help with cloning; **Funding**: Work in the Kjos lab is supported by a FRIMEDBIO grant (project number 250976) and a JPIAMR grant (project number 296906) from the Research Council of Norway. Work in the Murray lab was supported by a grant from the Biotechnology and Biological Sciences Research Council (BB/P018432/1). Work in the Grossman lab was supported, in part, by the National Institute of General Medical Sciences of the National Institutes of Health under award number R37 GM041934 and R35 GM122538. Work in the Veening lab is supported by the Swiss National Science Foundation (SNSF) (project grant 31003A_172861), a JPIAMR grant (40AR40_185533) from SNSF, a Novartis Foundation grant (#17B064) and ERC consolidator grant 771534-PneumoCaTChER; **Authors Contributions**: C.G. and J.W.V. wrote the paper with input from all authors. C.G., S.S., M.E.A., Y.M.S., X.L., G.A.S., S.P., R.R., J.D. and M.K. performed the experiments. C.G., S.S., M.E.A., M.K., H.M., S.G., A.D.G. and J.W.V designed, analyzed and interpreted the data; **Competing interests:** Authors declare no competing interests; **Data and materials availability:**All data is available in the main text or the supplementary materials. Genomes sequences are available at SRA PRJNA564501.

Supplementary Materials:

Materials and Methods

Figures S1-S5

Tables S1-S3

Movies S1-S8

Data S1